Journal of Semiconductors
JOS iopscience.iop.org/jos
www.jos.ac.cn

Accelerating hybrid and compact neural networks targeting perception and control domains with coarse-grained dataflow reconfiguration

Zheng Wang, Libing Zhou, Wenting Xie, Weiguang Chen, Jinyuan Su, Wenxuan Chen, Anhua Du, Shanliao Li, Minglan Liang, Yuejin Lin, Wei Zhao, Yanze Wu, Tianfu Sun, Wenqi Fang, and Zhibin Yu

Citation: Z Wang, L B Zhou, W T Xie, W G Chen, J Y Su, W X Chen, A H Du, S L Li, M L Liang, Y J Lin, W Zhao, Y Z Wu, T F Sun, W Q Fang, and Z B Yu, Accelerating hybrid and compact neural networks targeting perception and control domains with coarse-grained dataflow reconfiguration[J]. *J. Semicond.*, 2020, 41(2), 022401.

View online: https://doi.org/10.1088/1674-4926/41/2/022401

ARTICLES

Journal of Semiconductors
(2020) 41, 022401
doi: 10.1088/1674-4926/41/2/022401

Accelerating hybrid and compact neural networks targeting perception and control domains with coarse-grained dataflow reconfiguration

Zheng Wang[1, †], Libing Zhou[2], Wenting Xie[2], Weiguang Chen[1], Jinyuan Su[2], Wenxuan Chen[2], Anhua Du[2], Shanliao Li[3], Minglan Liang[3], Yuejin Lin[2], Wei Zhao[2], Yanze Wu[4], Tianfu Sun[1], Wenqi Fang[1], and Zhibin Yu[1]

[1]Shenzhen Institutes of Advanced Technology, Chinese Academy of Sciences, Shenzhen 518055, China

[2]School of Microelectronics, Xidian University, Xi'an710071, China

[3]School of Information and Communication, Guilin University of Electronic Technology, Guilin 541004, China

[4]Changzhou Campus of Hohai University, Changzhou 213022, China

Abstract: Driven by continuous scaling of nanoscale semiconductor technologies, the past years have witnessed the progressive advancement of machine learning techniques and applications. Recently, dedicated machine learning accelerators, especially for neural networks, have attracted the research interests of computer architects and VLSI designers. State-of-the-art accelerators increase performance by deploying a huge amount of processing elements, however still face the issue of degraded resource utilization across hybrid and non-standard algorithmic kernels. In this work, we exploit the properties of important neural network kernels for both perception and control to propose a reconfigurable dataflow processor, which adjusts the patterns of data flowing, functionalities of processing elements and on-chip storages according to network kernels. In contrast to state-of-the-art fine-grained data flowing techniques, the proposed coarse-grained dataflow reconfiguration approach enables extensive sharing of computing and storage resources. Three hybrid networks for MobileNet, deep reinforcement learning and sequence classification are constructed and analyzed with customized instruction sets and toolchain. A test chip has been designed and fabricated under UMC 65 nm CMOS technology, with the measured power consumption of 7.51 mW under 100 MHz frequency on a die size of 1.8 × 1.8 mm^2.

Key words: CMOS technology; digital integrated circuits; neural networks; dataflow architecture

Citation: Z Wang, L B Zhou, W T Xie, W G Chen, J Y Su, W X Chen, A H Du, S L Li, M L Liang, Y J Lin, W Zhao, Y Z Wu, T F Sun, W Q Fang, and Z B Yu, Accelerating hybrid and compact neural networks targeting perception and control domains with coarse-grained dataflow reconfiguration[J]. *J. Semicond.*, 2020, 41(2), 022401. http://doi.org/10.1088/1674-4926/41/2/022401

1. Introduction

Recent advancements in neural networks have demonstrated their success in a wide range of application domains, such as computer vision, natural language processing, and gaming engines. Although questions still exist on the appliance of neural networks into further domains, there is inarguably the increasing demand on the computing power to support fast-evolving network structures.

Traditionally, neural networks are mostly deployed on CPU and GPU-based platforms, resulting in either less computing performance or huge power consumption. Recently, the CPU-FPGA based heterogeneous programming paradigm has also appeared to support higher performance. However, both solutions suffer from extensive power consumption caused by a significant amount of data movement between computing elements. Dedicated hardware accelerators have been proposed to accelerate the inference phase of neural networks such as Eyeriss[1], Google TPU-I[2] and DaDianNao[3]. Such highlighted architectures achieve high performance and resource utilization with specific algorithmic-architecture co-design techniques, such as row-stationary dataflow and systolic array matrix multipliers. The majority of hardware optimization techniques are proposed for the standard convolution kernel, which accounts for 90% computing operations of the state-of-the-art neural networks[4]. Accelerator supporting both convolutional and recurrent algorithmic kernels has been proposed in Ref. [5] with optimization techniques on bit-width and pattern access, which opens the research direction on architecture for advanced hybrid neural networks.

Standard convolution plays a key role in feature extraction, its amount of computation and network parameters have been increasing rapidly[6], which poses severe challenges in deploying standard CNNs on embedded and mobile devices. To address this, recently compact CNNs such as SqueezeNet[7] and MobileNet[8] have been designed to drastically reduce the total amount of computation while maintaining similar accuracy compared to standard CNN models. For instance, MobileNet reduces 27 × in computation and 32 × in parameter size but only degrades 1% in accuracy compared to VGG-16[9]. Conventional optimization techniques in neural accelerators are less generalizable to compact kernels. For instance, Winograd[10] and FFT-based[11] transformations are efficient for 3-D filters but ineligible for pointwise (PW) convolution. Additionally, depthwise (DW) convolution has a low computation to communication (CTC) ratio[12], which makes it diffi-

Correspondence to: Z Wang, zheng.wang@siat.ac.cn
Received 8 OCTOBER 2019; Revised 16 DECEMBER 2019.

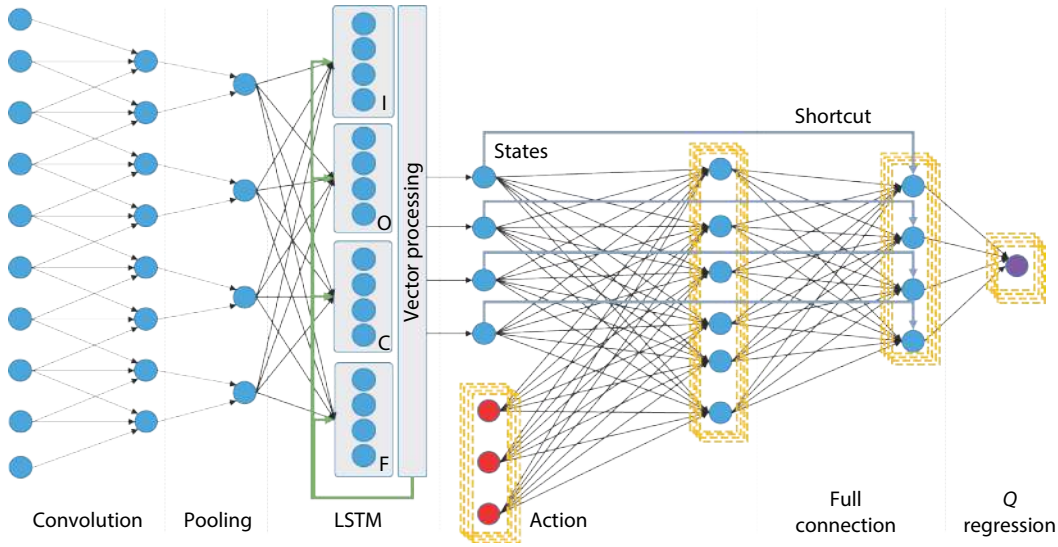

Fig. 1. (Color online) Structure of hybrid neural network targeting perception and control with layer-wise algorithmic kernels.

cult to be executed as efficient as standard convolution.

On the other hand, the AI community has also witnessed the applications of neural networks in non-perceptual domains such as decision-making. In the domain of control systems, decision making through deep reinforcement learning has shown progressive achievements. The deep Q network (DQN), which was originally proposed in Ref. [13], uses multi-layer neural networks to implement the *Q*-function in order to eliminate the lookup-table for storing *Q*-values. Deepmind demonstrates a ground-breaking contribution in Ref. [14] by combining CNN and DQN to realize beyond human-level performance in Atari gaming. AlphaGo[15] and Zero[16] are designed with deep reinforcement learning kernels as well. Despite its increasing importance, current hardware accelerators have very few supports for control-related kernels.

Consequently, there is a high probability that future neural networks are capable of performing end-to-end tasks in perception, control, and even actuation with hybrid, compact algorithmic kernels. However, current dataflow techniques such as weight-stationary (WS), output-stationary (OS) and row-stationary (RS)[17] only targets for fine-grained data reuse of standard convolution. To achieve both functional support and high resource utilization, accelerator designers should analyze characteristics of various kernels, such as data flow and access patterns, functionalities of computing resources, while minimizes the control and synchronization overheads among thousands of processing elements (PEs). In this work, we propose a reconfigurable dataflow processor, which adjusts the patterns of data flowing, functionalities of processing elements and on-chip storages according to network kernels, including standard and compact convolution, pooling, full connection, shortcut, long short-term memory (LSTM)[18] and state-action layer in DQN. The proposed architecture increases resource utilization across multiple kernels through coarse-grained management of dataflow, which is complementary to other fine-grained techniques. A dedicated instruction set and toolchain have been built to manage dynamic reconfiguration and achieve compatibility with mainstream AI programming environments. A reconfigurable ASIC has been designed and fabricated under 65 nm CMOS technology, with a measured power consumption of 7.51 mW under 100 MHz frequency on a 1.8 × 1.8 mm^2 die size.

2. Data flow for neural network kernels

2.1. Standard kernels

Fig. 1 visualizes important network layers and their interconnections, which form an end-to-end network targeting both perception and control. Especially for graphical input, concatenated convolution and pooling layers are applied as perceptional building blocks for extracting visual features. Model networks such as Yolo-v3 and Resnet-50 can have tens of such layers, imitating the human visual system. For timing sequence-dependent applications, such as video context understanding and language processing, sequences of extracted features through time are provided as input to the LSTM layer, which extracts sequence-dependent features. Opposed to former layers, LSTM constitutes four basic gates, naming input (I), output (O), cell state (C) and forget (F) gates. While I, O and F gates compute layer output through vector operations, C gate keeps the current layer states which are also provided as recurrent input for the next sequence in time.

The control network starts after feature extraction layers. In DQN, the extracted features are treated as nodes of states, while the optimal decision needs to be chosen through nodes of actions. The approach is to iterate through all possible actions under current states and perform regression to find maximal or minimal output value (*Q* value) depending on strategies of reinforcement learning. The procedure is represented as a state-action layer in Fig. 1. Since action nodes need to be iterated, all computation in the following layers needs to be iterated as well, represented as yellow dash boxes. The fully connected layer is prevalent since the invention of the multi-layer perceptron. However, shortcut links are often used, especially in residue networks, to improve the accuracy of classification and regression by providing features form layers before the current input.

Various layers differ not only in the network structures, but also operands, operators, nonlinear functions. Table 1 summarizes the characteristics of multiple kernel layers. It is observed that pooling and shortcut operate on vectors while oth-

Table 1. Operation characteristics among multiple standard neural network kernels.

NN Layer	Convolution	Pooling	FC	LSTM	State-action	Shortcut
Operands	Sparse matrix	Vector	Dense matrix	Dense matrix	Dense matrix	Vector
Operators	Sum of product (SoP)	Max, min, mean	SoP	SoP vector multiply vector sum	SoP	Vector sum
Nonlinear functions	ReLU sigmoid	None	ReLU sigmoid	Sigmoid tangent	ReLU sigmoid	None
Dataflow property	Serial in/out thread-level parallelism	Parallel in/out	Serial in/out thread-level parallelism	Serial in/out shared among gates	Serial in/out action nodes iteration	Parallel in/out
Buffering property	Activation dominant	Activation dominant	Weight dominant	Weight, states	Weight, states, actions	Activation pointer

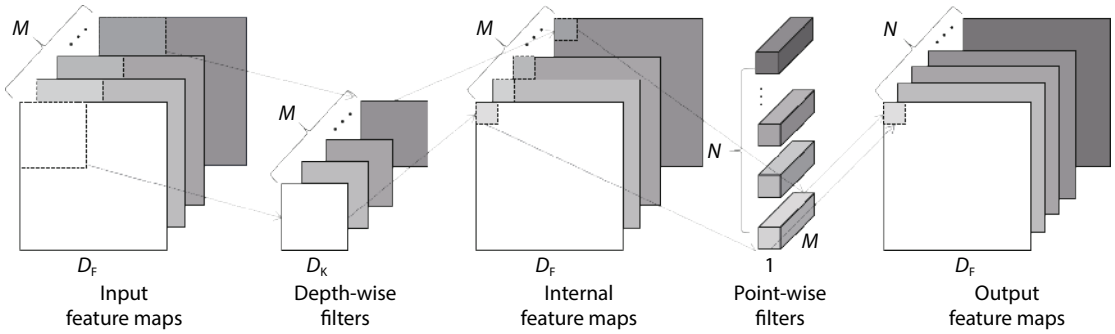

Fig. 2. Orientation and dimensions of compact CNN filters.

er kernels operate on matrix, among which convolution processes sparse matrix and the rest kernels process dense matrix. Concerning nonlinear functions, LSTM adopts simultaneously sigmoid and tangent while the rest matrix kernel uses either ReLU or sigmoid.

The dataflow properties are generalized from network structure. In convolution and fully connected layers, activations (network data) need to be shared among nodes of the output feature map. LSTM adopts similar serial streaming with the special case that activation streams need to be shared among multiple gates. The state-action layer, on the other hand, requires fast data flow generation based on the iteration of action nodes. Pooling and shortcut which operate on vectors do not need to share activation for feature maps. Therefore vector types of activation can be streamed in parallel.

Furthermore, we analyze the functionality of the intermediate data used in multiple kernels. Due to the nature of data sparsity, convolution and pooling are dominant by activations, while on the contrary, FC and LSTM are dominant by weights. LSTM and State-action contain generated data for cell states and actions, respectively. In the shortcut layer, pointers to activations of the previous layer need to be bookkept, for the network to address previous data.

2.2. Compact convolutions

The essences of compact CNNs are depthwise (DW) and pointwise (PW) convolution. As shown in Fig. 2, DW convolution utilizes a unique 2-D filter to convolve data within a single input channel. PW convolution, on the other hand, applies a 1-D filter to perform linear combination across multiple channels. We label the dimension of input feature map (Ifmap) by $D_F \times D_F \times M$ where D_F is the spatial height and width, M is the number of input channels. The output feature map (Ofmap) after DW convolution has the dimension of $D_F \times D_F \times M$, which is passed onto PW convolution as Ifmap.

Table 2. Number of operations of standard, DW and PW convolution layers.

Layer	Filter size	Input size	MAC amounts
Standard conv	$D_K \times D_K \times M \times N$	$D_F \times D_F \times M$	$D_K \cdot D_K \cdot M \cdot N \cdot D_F \cdot D_F$
Conv DW	$D_K \times D_K \times M$	$D_F \times D_F \times M$	$D_K \cdot D_K \cdot M \cdot D_F \cdot D_F$
Conv PW	$1 \times 1 \times M \times N$	$D_F \times D_F \times M$	$M \cdot N \cdot D_F \cdot D_F$

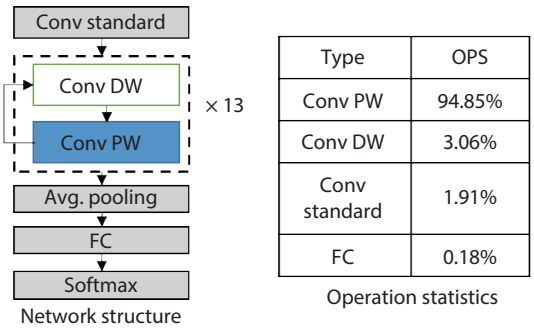

Fig. 3. (Color online) Structure and operation distribution for MobileNet.

The Ofmap of PW convolution is $D_F \times D_F \times N$. The number of operations compared to standard convolution is present in Table 2, which is evaluated in the number of multiply-and-accumulation (MAC). For the typical D_K value of three, replacing standard convolution with DW and PW convolution leads to MAC reduction up to 90%[9].

Fig. 3 visualizes the MobileNet structure, which concatenates several network layers. Besides standard convolution, pooling, FC and softmax layers that are available in conventional CNN, thirteen repeated blocks of DW and PW convolution play a crucial role in network organization. As shown in the statistics chart, 94.85% of total operations in MobileNet is PW convolution while DW convolution ranks the second by

3.06%. Other compact CNNs follow similar statistics of operations, which indicates massive demand in the acceleration of PW and DW convolution.

3. Reconfigurable dataflow processor

According to the analysis of algorithmic kernels on Section 2, a dataflow processor is designed to achieve dynamic functional reconfiguration through coarse-grained dataflow management. This section describes the design methodology, micro-architecture, instruction set architecture, and associated toolchain for model conversion from mainstream deep learning frameworks.

3.1. Methodology of dataflow reconfiguration

To implement standard algorithmic kernels in Table 1 and possibly save hardware resources, the design of reconfigurable architecture should at least cover the union of different kernels. To achieve this, the resources are maximally shared among kernels, including PEs, data input/outputs, buffering SRAMs and DRAM interfaces. Fig. 4 illustrates the methodology of data flow management and resource sharing, which is also explained as the following:

Convolution: PEs, which are configured as MAC and ReLU in function, are grouped in multiple threads, where each thread processes data with the same row and column across multiple channels of the output feature map. SRAMs are mostly used for buffering thread dependent activations of the input feature map. Weights are shared across multiple threads. Activations are serially streamed from the individual buffer to achieve sharing among PEs. Serial outputs from individual threads are associated in the output buffer and streamed out in parallel through SERDES and DRAM controller.

Pooling: PEs are configured as a comparator to achieve max and min operators. Since pooling operates on vectors, the activations fetched from DRAM are directly provided to PE arrays without buffering, which extensively saves dynamic power consumption. Both parallel input and output are utilized. Activations are compared through time by modifying DRAM access addresses.

Full connection: for such weights dominant kernel, SRAMs are configured as weight buffers while activations are serially streamed through multiple threads. Outputs and PE configurations are similar to convolution.

Shortcut: Similar to pooling, the kernel works on vectors. The PEs are configured as an addition. Since two vectors are added, both input and output shift registers are used to store operands, which results are written to the output shift registers and written to DRAM in parallel. The pointer buffer is instantiated to address both operands in DRAM.

LSTM: PEs are grouped into four sets of gates which each set instantiates different nonlinear functions between sigmoid and tangent. Additional vector operators and tangent modules are used for post-processing. A mixed-mode input style is adopted for both activation sharing within each set of gates and fast data provision among different sets. Cell state buffer is instantiated to keep intermediate state information.

State-action: input/outputs and PE configurations are similar to full connection. Multiple origins of activations exist, including DRAM for conventional activations, on-chip buffering for activations of states and iterative actions.

Fig. 5 illustrates the proposed flow of data streaming for compact convolutions. Activations are associated into bundles. Each bundle has the size of a single read transfer of DRAM memory, which is eight bytes here for instance. Activations in the bundle are executed in parallel on multiple hardware threads. For PW convolution, bundle groups horizontal data elements. Burst read mode of DRAM streams eight input threads of data bundles vertically and simultaneously computes eight output threads. Showing in Fig. 5, with only four streams the Ofmap with the size of 16×16 is ready to commit. On the contrary, for DW convolution, bundle vertically groups eight data elements and streams horizontally. After streaming multiple rows of Ifmap depending on the filter dimension, bundles of multiple data in Ofmap are ready to commit. The grouping and streaming directions are in orthogonal to the filter dimension, which maximally exploits computing parallelism.

The alternating direction of streaming and committing is designed to cater to the nature of alternating PW and DW layers in compact CNN. Therefore, no extra logic and cycles are required to re-arrange data alignment, which achieves a high saving in execution time and hardware cost.

3.2. Microarchitecture

The microarchitecture of the proposed reconfigurable dataflow processor is illustrated in Fig. 6. It employs a hierarchical design methodology, including PE, hardware thread and system-on-chip. This subsection introduces the individual module and its design considerations.

System-on-chip: this abstraction performs system-level coordination of individual threads and PEs. It is composed of four subsystems: execution controller, direct memory access (DMA) controller, execution threads, and buffers.

The execution controller mainly coordinates PEs and buffers according to network instructions. Upon initialization, it fetches instructions from DRAM into configuration SRAM, sequentially decodes each instruction and drives execution threads to achieve targeting network functions. A centralized control methodology is adopted to reduce logic overheads and boost performance.

The DMA controller achieves multiple modes of reads and writes between SoC and external DRAM storage. It fluently transmits network configurations, weights, activations, and results. DDR burst mode is considerably adopted to rapidly provide data and reduce DRAM access power. It is well-known that memory bandwidth incurs limitation to the computational throughput. Hence, we design the DMA according to the algorithmic properties, specified in Section 3. For instance, the data bundle for PW and DW convolution has the size of elements equaling to the number of bytes per transfer under a specific DRAM protocol. Therefore continuously burst read and write are possible without further data buffering.

A pool of SRAM buffers is designed where each SRAM has 8 KB size. The analysis in Section 3 inspires the SRAM pool structure, where different algorithmic kernels have divergent usage of buffering. With the assistance of the execution controller, the SRAM is instantiated into various buffering functions on the fly, determined by algorithmic kernels. For detailed usage of the SRAM pool, please refer to buffering properties in Table 1.

Hardware threads: this design abstraction is introduced for easy management of resource sharing for both data flow

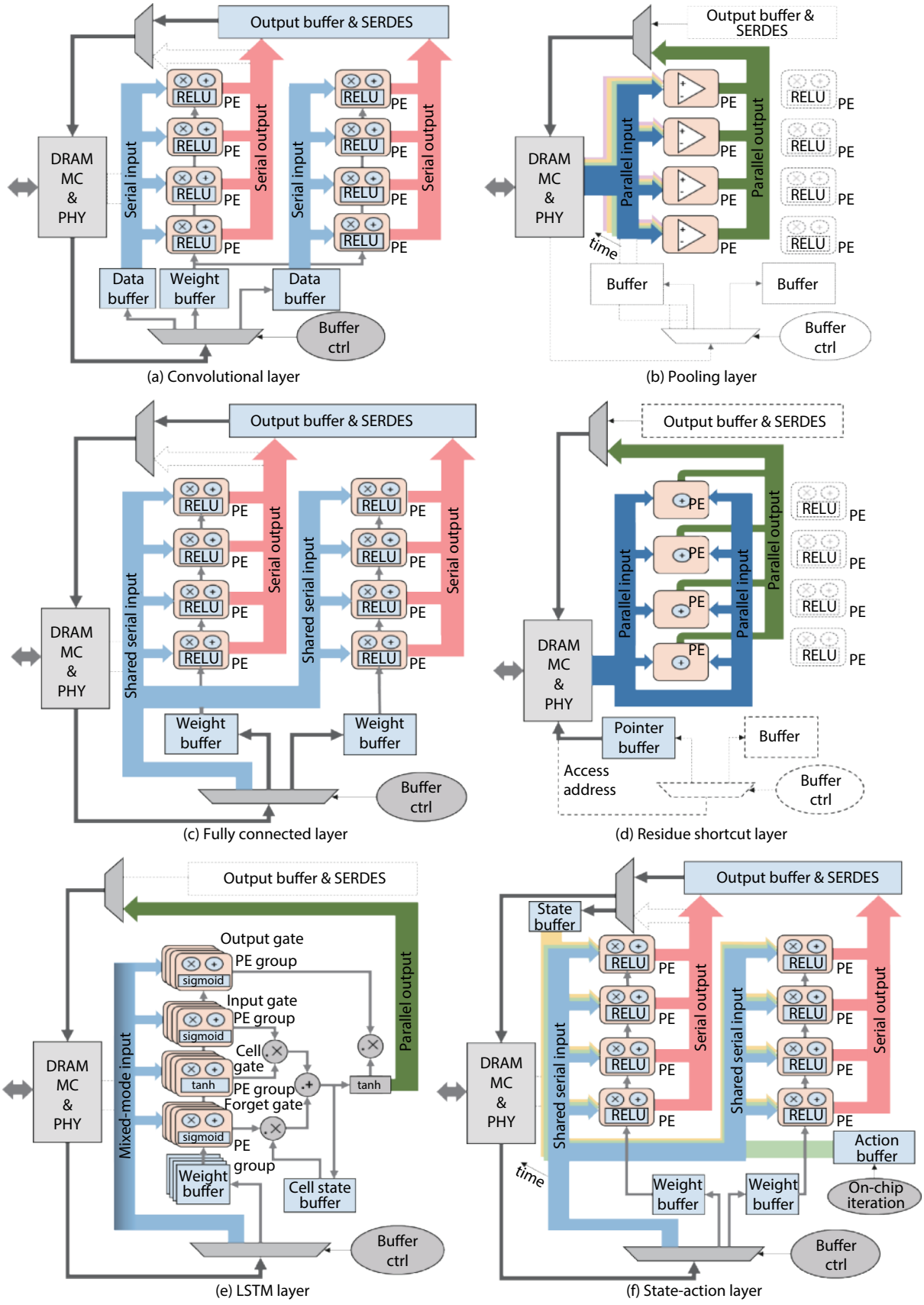

Fig. 4. (Color online) Reconfiguration of dataflow, PE and storage functionalities for standard kernels.

and weights. Activation inputs and outputs are built using shift registers to achieve both data sharing and fewer power overheads due to single fan-out and reduced load capacitances. Shift registers can be dynamically configured as serial and parallel modes according to Fig. 4. In contrast to the single direction of the in-data stream, the out-data stream is bidirectional to facilitate vector computation used in shortcut kernel. Multiple PEs are coordinated through thread-level finite state machine (FSM) to process activations and weights in a pipeline fashion. The weights are streamed-in from the

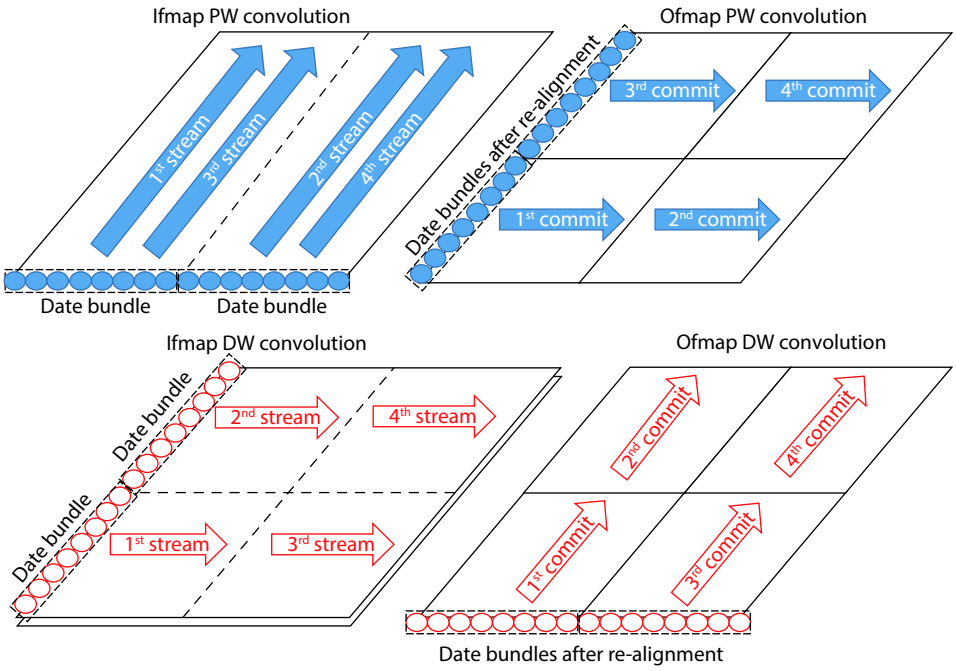

Fig. 5. (Color online) Reconfiguration of dataflow for pointwise (PW) and depthwise (DW) convolution kernels.

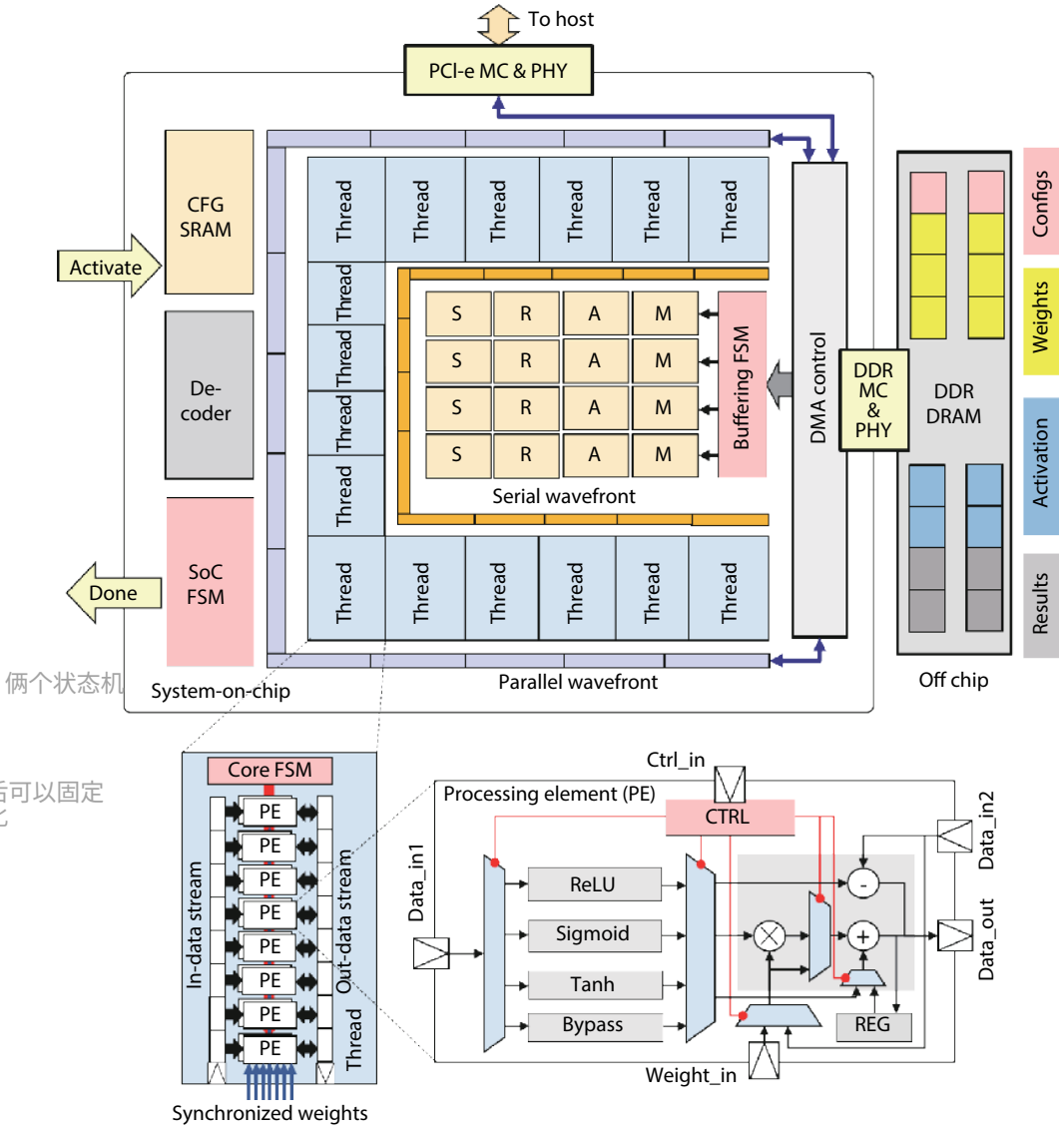

Fig. 6. (Color online) Microarchitecture of proposed reconfigurable dataflow processor.

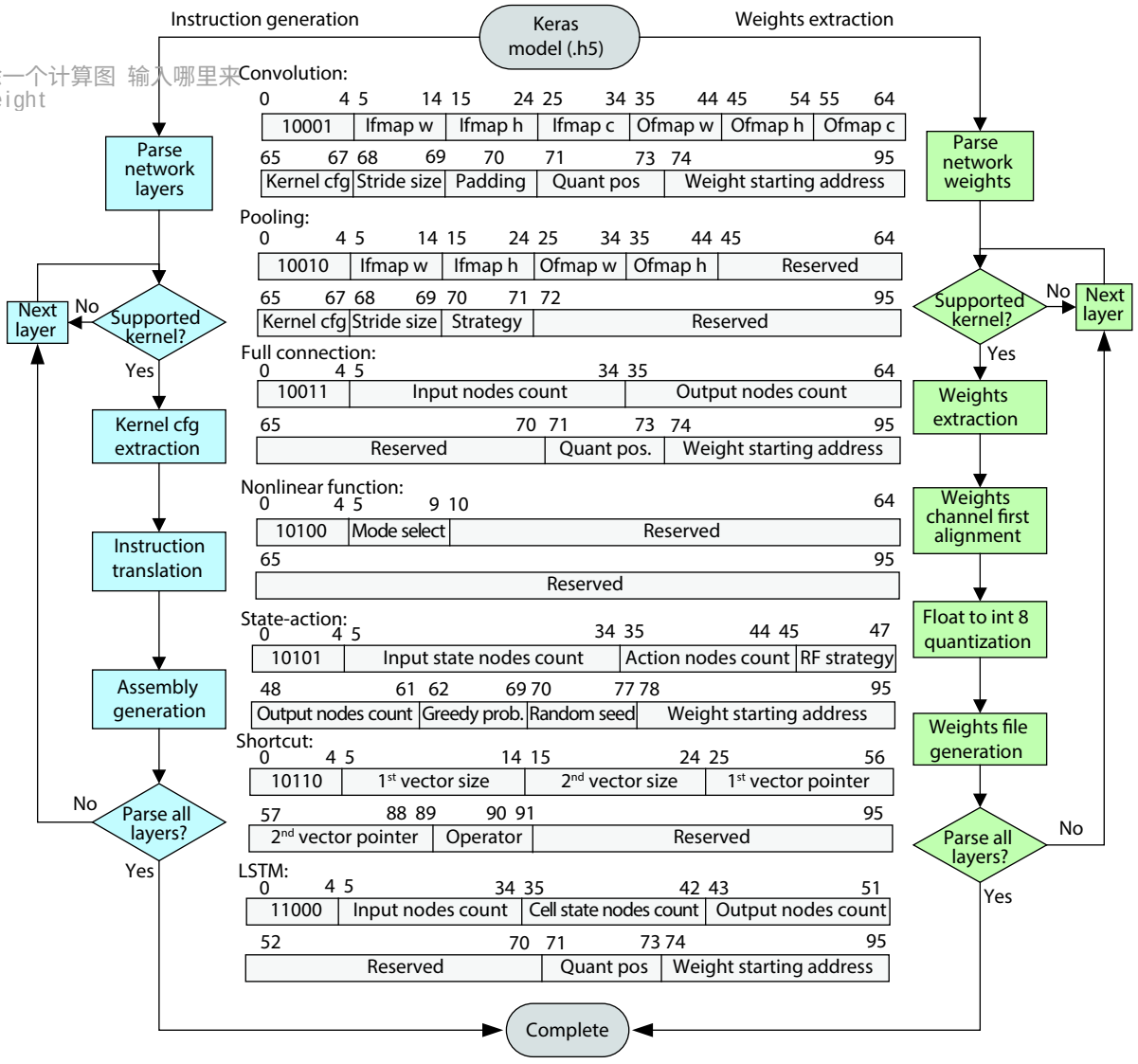

Fig. 7. (Color online) Instruction set architecture (ISA) and developing toolchain.

SRAM pool in the SoC, where individual PEs can receive different weight streams.

Processing elements: To efficiently compute kernel-dependent functions, PE is compactly designed to achieve required operators. It facilitates both matrix and vector computation through both data input ports and one weight input port. The Sigmoid and Tangent modules are designed based on the linear approximation technique in Ref. [19]. The control input receives opcode from thread-level FSM to configure multiplexers to realize kernel-dependent operators.

3.3. Instruction set and toolchain

Customized instruction set architecture for the proposed processor is designed, supporting neural network algorithmic kernels in Section 3. As shown in Fig. 7, instructions have a length of 96 bits and contain divergent fields across instruction types. In general, the proposed ISA specifies the operator (opcode in first five bits), properties of input and output operands, quantization bit for activation and weight addressing index from DRAM. Address for activation is not necessary for the majority of layers since the following layer reads activations from the previous layer by default.

For convolution and pooling, dimension descriptions on Ifmap, Ofmap, and filters are specified, as well as stride and padding properties. Convolution modes of standard, PW and DW are automatically decoded in micro-architecture according to filter dimensions. Pooling instruction contains the strategy field for choosing between max, min, and average pooling.

The nonlinear function layer can be specified among ReLU, sigmoid, tangent, and bypass. The state-action layer contains an extra field for size of action nodes, strategy selection, plus the probability of random action taking (epsilon greedy) and associated random number seed. The details of DQN architecture and controlling strategy is referred to Ref. [20].

The shortcut layer operates on two vector operands; hence, their activation addressing (pointer) and sizes need to be specified in the instructions. LSTM layer contains fields of sequence-dependent cell state nodes besides regular input nodes.

The design methodology of the proposed architecture favors an ASIC design manner instead of a CPU centric one. Typically ASIC adopts a finite state machine for control flow instead of RISC-style instructions in the CPU. The instruction or configuration in ASIC tends to guide the state transition from higher abstraction, to realize the design of multi-mode func-

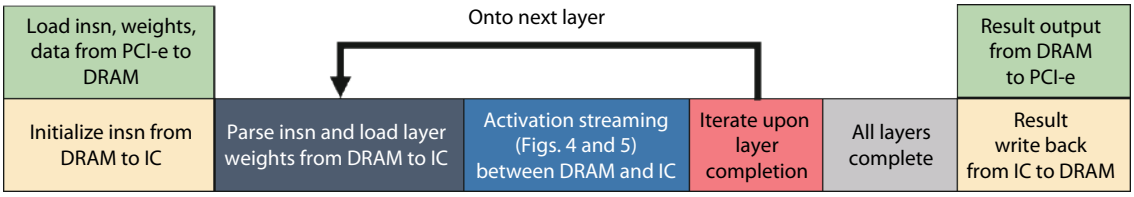

Fig. 8. (Color online) Operational phases of proposed architecture.

tional circuits. Consequently, the customized layer-wise instructions facilitate data stream reconfiguration according to Figs. 4 and 5. Compared to traditional RISC style ISA, such high-level ISA constructs the abstraction layer which leaves fine-grained operation management to the controller state machine in the processor and significantly simplifies the compilation flow of neural networks.

The developing tool flow converts the state-of-the-art network model to deployable format on proposed architecture. Taking Keras network h5 model[21] for instance, two separate branches of toolchains generate network instructions and weights by converting corresponding members. For unconvertible instruction such as a state-action layer, a graphical interface has been designed for manual input of network specifications. For weights conversion, the proposed architecture adopts channel last data alignment for both weights and activation to improve performance[22] and approach in Ref. [23] for statistical quantization of layer-wise activations. The reason for the separate flow of weight preparation is to modify the standard weight format for maximal usage of DRAM burst access mode in order to reduce memory access power and latency. After the format transformation of weights, the architecture exploits simple burst-based streaming instead of sophisticated data flow management.

3.4. Operation management

The internal finite state machine contains more than 100 states for activation/weight buffering, synchronization of multiple threads and processing with high utilization of PEs. For brevity, the FSM is not explicitly described in this section. Instead, phases of operations are summarized below and also presented in Fig. 8.

Initialization phases: Such phases load network instructions, weights and input activation from the host machine to DRAM of the processor with specific locations for all three types of data. The interface with the host can be one of the SERDES such as PCI-e. Afterwards, the instructions are loaded from DRAM to CFG buffer in the SoC. Currently an 8 kB size of CFG buffer is deployed to hold a maximum of 682 layer network instructions, which is sufficient for mainstream artificial neural networks.

Computation phases: The SoC controller fetches, decodes each network instruction and reconfigures the dataflow according to Figs. 4 and 5. The duration of reconfiguration takes only eight clock cycles including fetch and decode. Subsequently, weights for corresponding network layer and input activations are streamed into individual threads and processed by PEs. Weights and activations are streamed with an interleaved manner to maximally exploit the length of burst access of DRAM. Once upon completion of the network layer, the controller iterates onto the next layer and continues reconfiguration and data streaming. Intermediate results are streamed to and from DRAM without external manipulation.

Output phases: When the last network layer is complete, the controller streams multiple batches of results to DRAM. Once all results are available, they are streamed from DRAM to host through SERDES. The next batch of input activations is ready to be streamed-in after the output of the current result.

4. Experiments

4.1. Design methodology

The demonstrated architecture with 108 kB on-chip SRAMs and 16 PEs fitting in one single thread is designed completely in Verilog and simulated using Modelsim to characterize performance on individual network kernels. Logic synthesis by Design Compiler is carried out under UMC CMOS 65 nm low-leakage technology library. Placement and routing are performed by Innovus to generate layout. Calibre is for physical verification and sign-off. The prototype chip has been fabricated by UMC through a multi-project wafer (MPW) service provided by Europractice.

Currently, IPs for DRAM and PCI-e interfaces are missing in the taped-out chip. To verify the designed DMA controller and DRAM data access, simulation models of 512 MB DDR3 DRAM, memory controller and PHY (MIG) are generated using Xilinx ISE with a DQ width of 16 bits and DDR frequency of 800 MHz. Opal Kelly Frontpanel technology[24] is used to replace the PCI-e IP for interfacing with the host machine through FPGA.

The exemplary design on FPGA contains 256 PEs fitting in 16 hardware thread, 18 × 6 kB on-chip SRAM buffers, including 16 reconfigurable SRAM blocks, one configuration SRAM and one special purpose SRAM. The dimensions of PEs and SRAMs are chosen to match the data width provided by the DRAM for better utilization of off-chip memory bandwidth.

Toolchains for network model conversion is developed in Python. Currently, the Tensorflow Keras h5 model is supported, while integration with Caffee and Darknet frameworks are under development. After DRAM calibration, converted network configuration, inputs, and weights are downloaded into specific address spaces in DRAM through Frontpanel and DMA controller in the SoC. Upon completion of model downloading, the SoC begins layer-wise processing according to reconfigurable dataflow described in Section 3. Benchmarks are chosen from Keras framework in Python and neural network toolboxes in MATLAB.

4.2. Performance analysis

Three network structures have been demonstrated to analyze the performance of the proposed architecture: First, MobileNet with hybrid kernels of standard, PW and DW convolutions, pooling and full connection. Second, maze walk-

Table 3. Benchmark of performance for MobileNet with proposed architecture[25].

Layer type	Input size	#. MACs	Multi-threaded streaming architecture @ 100 MHz					Single-threaded latency (ms)[24]
			Max BW utilization	Max PE utilization	#. stream	ns / stream	Latency (ms)	
Conv0 Std.	224 × 224 × 3	10.84M	3%	6.70%	25088	3340	83.8	83.8
Conv1 DW	112 × 112 × 32	3.61M	10%	6.70%	25088	2080	17.4	380.5
Conv1 PW	112 × 112 × 32	25.69M	100%	100.00%	3136	1835	5.8	92.1
Conv2 DW	112 × 112 × 64	1.81M	10%	6.70%	12544	2080	8.7	190.2
Conv2 PW	56 × 56 × 64	25.69M	100%	100.00%	1568	3520	5.5	88.3
Conv3 DW	56 × 56 × 128	3.61M	10%	6.70%	25088	2080	17.4	380.5
Conv3 PW	56 × 56 × 128	51.38M	100%	100.00%	1568	6890	10.8	172.9
Conv4 DW	56 × 56 × 128	0.90M	10%	6.70%	6272	2080	4.3	95.1
Conv4 PW	28 × 28 × 128	25.69M	100%	100.00%	784	6890	5.4	86.4
Conv5 DW	28 × 28 × 256	1.81M	10%	6.70%	12544	2080	8.7	190.2
Conv5 PW	28 × 28 × 256	51.38M	100%	100.00%	784	13630	10.7	171
Conv6 DW	28 × 28 × 256	0.45M	10%	6.70%	3136	2080	2.2	47.6
Conv6 PW	14 × 14 × 256	25.69M	100%	100.00%	416	13630	5.7	90.7
Conv7-11DW	14 × 14 × 512	0.90M	10%	6.70%	6272	2080	4.3	95.1
Conv7-11PW	14 × 14 × 512	51.38M	100%	100.00%	416	27110	11.3	180.4
Conv12 DW	14 × 14 × 512	0.23M	10%	6.70%	1568	2080	1.1	23.8
Conv12 PW	7 × 7 × 512	25.69M	100%	100.00%	256	27110	6.9	111
Conv13 DW	7 × 7 × 1024	0.45M	10%	6.70%	3136	2080	2.2	47.6
Conv13 PW	7 × 7 × 1024	51.38M	100%	100.00%	256	54070	13.8	221.5
Avg Pool	7 × 7 × 1024	0.05M	10%	6.70%	64	1767	0.1	0.1
FC	1 × 1 × 1024	1.02M	55%	6.70%	63	90218	5.7	5.7
Total	—	569M	—	—	—	—	294.3	3856.5

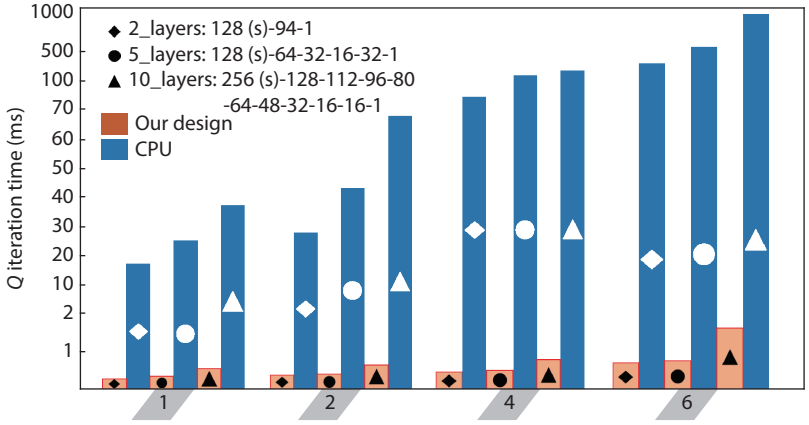

Fig. 9. (Color online) Comparison of *Q* iteration time between proposed architecture and host machine (CPU)[27].

through by DQN with state-action and full connection kernels. Third, sequence classification with hybrid kernels of LSTM and full connection.

MobileNet: As introduced in Section 2.2, MobileNet adopts iteratively compact convolution kernels, which account for 97.91% of computation in the number of MACs. Table 3 shows the profiled execution latency of proposed design throughout various layers of MobileNet, benchmarked between multi- and single-threaded architecture, using an FPGA prototype with 256 PEs and DRAM support.

The total network latency with multi-threading is only 7.6% of the single-threaded design proposed in Ref. [22] under the same frequency of 100 MHz. Such acceleration is mainly due to the following factors. In DW convolution, maximal utilization of DRAM bandwidth and processing elements do not reach a high level. However, the 2-D filters across multiple channels are fetched from DRAM in a burst manner and computed with data elements of a bundle in parallel, which consequently leads to a 21.9× saving of latency. On the other hand, PW convolution achieves a 16× speed-up due to maximal 100% usage of memory bandwidth and PEs, which is only possible with the assist of continuously addressed data bundles in burst mode.

Besides compact convolution layers, the first layer of standard convolution is processed only in the single thread due to the irregular addressing for three channel RBG feature maps, which incurs only 6.7% of PE utilization. Ongoing work is targeting the issue of irregular addressing with multi-functional on-chip SRAMs. The pooling layer is executed with parallel input and output stream on a single thread as shown in Fig. 4(b). A fully connected kernel utilizes 16 PEs similar to a single-thread design. The parallelism is limited by the fact that the weight stream for individual output node in the FC layer cannot be shared among PEs and noted that the pro-

Table 4. Benchmark of performance for LSTM networks among three processing architectures.

Network layer specification	1st LSTM layer	2nd LSTM layer (if need)	1st FC layer (if need)	2nd FC layer
	In nodes: 3, Out nodes: 12, Recurrent nodes: 48	In nodes: 12, Out nodes: 12, Recurrent nodes: 48	In nodes: 12, Out nodes: 12	In nodes: 12, Out nodes: 5
Network	Performance (ms/sample)			Average power consumption
	1 LSTM + 1 FC	2 LSTM + 1 FC	2 LSTM + 2 FC	
CPU Intel i7-8700 @3.20 GHz	11.981	22.362	23.962	60–70 W
CPU Intel i7 w. GPU NVIDIA GTX 1050	2.87	4.94	5.74	50–70 W
Proposed design with 16 PEs @ 100 MHz *	1.033	1.157	1.957	30–50 mW

* Simulation result, not account for data transferring between disk storage and DRAM.

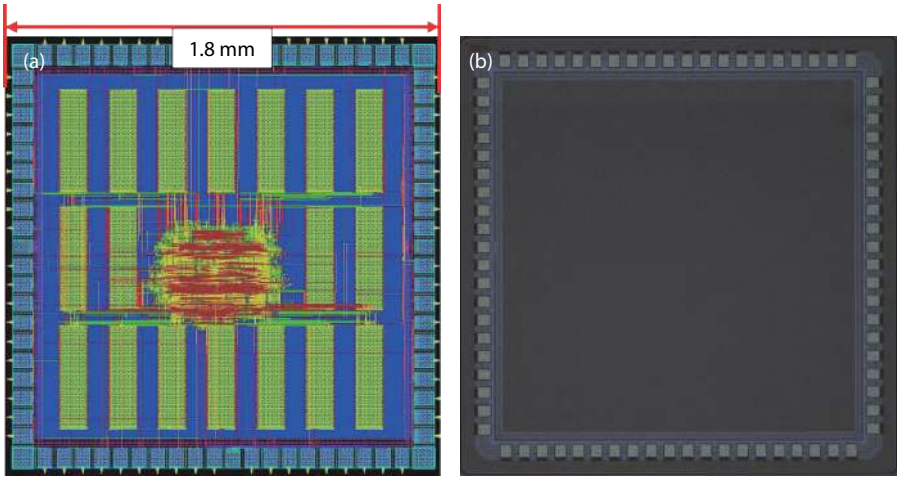

Fig. 10. (Color online) (a) ASIC layout with 16 reconfigurable PEs. Logics (middle) surrounded by 18 SRAM blocks. (b) Micrograph of taped-out chip with UMC CMOS 65 nm low-leakage technology.

cessing latency considers not only streaming of activation but also weights, which accounts for ~60% of latency for full connection.

Deep reinforcement learning: a typical usage of DQN is maze walking, where the intelligent agent learns to walk towards the destination by picking right directions at the crossroad and also avoiding barriers. To model maze walking with the state-action layer in DQN, the actions for the agent upon choices are modeled as discrete action nodes, where states are modeled with whether the agent's faces surrounded barriers in different directions. For details on modeling maze walking with DQN, the readers are referred to Ref. [26].

After modeling, we tune the sizes of state and action space and compare the computation time consumed by different structures of the DQN network and the dimensions of the action space. As shown in Fig. 9, one, two, four and six nodes of action space are tested on the 2-, 5-, and 10-layer network, while state space is chosen between 128 and 256 nodes. For all tested action space, the on-chip Q iterative time of all three network structures is less than 2 ms. Such iteration time slightly increases with the dimension of action space as well as the network size.

We profile the Q iteration time for the same configuration of network and action space on the host machine with the Intel i7 processor. MATLAB with Neural Network Toolbox with the feature of runtime profiling is used for benchmarking. As shown in Fig. 5, the proposed architecture with on-chip Q iteration achieves at least 100 × speed-up compared to the host machine for all configurations, demonstrating the advantage of the proposed architecture for decision network.

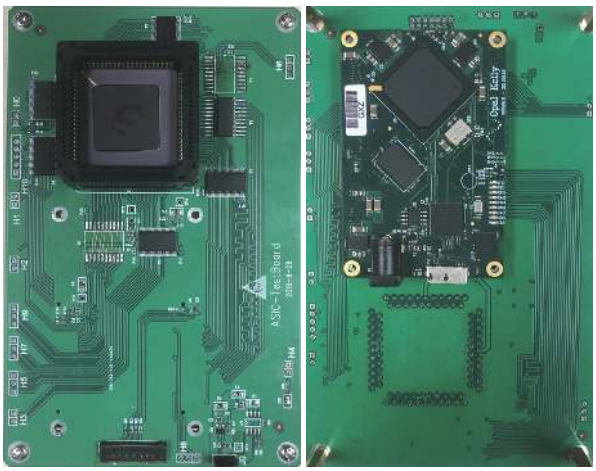

(a) Front view (b) Rear view

Fig. 11. (Color online) Views of the testing board. The front view contains testing IC under CLCC84 packaging and socket. The rear view contains FPGA for interfacing IC with the host machine.

Sequence classification: the testing example employs sensor data obtained from smartphone worn on the body[30]. The data is trained with an LSTM network to recognize the activity of the wearer given time series representing accelerometer readings in three different directions. The network combines the LSTM layer and full connection layer, followed by the Softmax layer for classification, where the first two layers are used for performance analysis.

Table 4 presents the testing network with layer-wise structure specifications. Performance is benchmarked on the

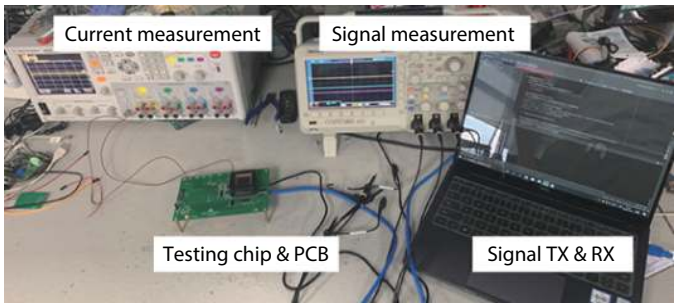

Fig. 12. (Color online) Testing infrastructure with measurement of both signal voltages and currents.

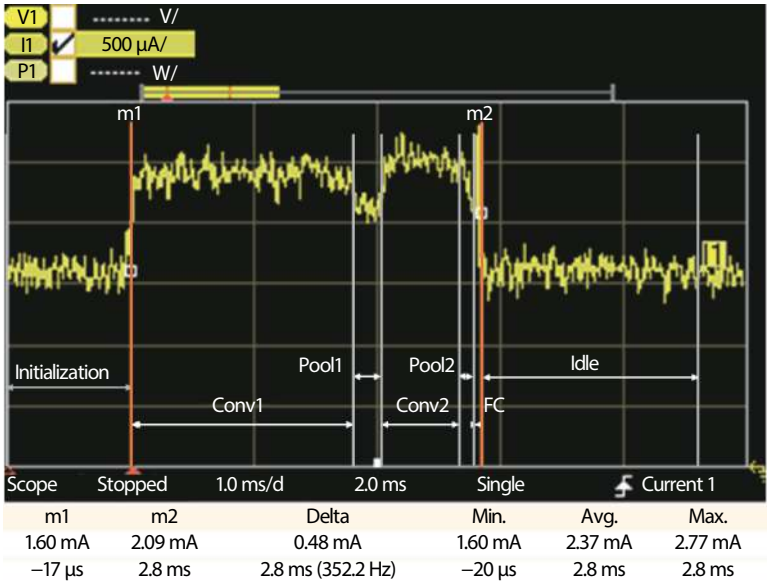

Fig. 13. (Color online) Runtime current measurement across different phases of operation under 30 MHz frequency.

following three platforms: Intel i7 CPU and NVIDIA GTX GPU with measured latency in MATLAB neural network toolbox and proposed design of 16 PEs with simulated latency in Modelsim. It is observed that for all network specifications, the proposed design achieves improved performance compared to CPU and GPU. It is noticed that the measurement results from MATLAB consider huge latency of data transfer between disk, main memory, and operating system, whereas our design is proposed as a standalone system. However, future LSTM networks tend to be deployed on sensors and process data directly from DRAM, which is close to the design principle of our design. CPU and GPU consume three orders of magnitudes higher power than the proposed design, proving the energy efficiency of ASIC for hybrid neural networks.

4.3. Physical results

The reconfigurable ASIC has been taped-out with UMC CMOS 65 nm low-leakage technology. Fig. 10 presents the chip's layout and micrograph. The ASIC has a die size of 1.8×1.8 mm^2 including 80 IO pads, 16 PEs, and 18 SRAM blocks. The driving voltage for the core and IO is 1.2 and 2.5 V respectively. The chip communicates with testing FPGA board using customized 8-bit input and output data ports.

Regarding the layout, SRAM IPs with 6 kB each occupy ~50% of the core's die area. The size of SRAM IP is chosen to fit the number of weights per channel of typical convolution Ofmap (Up to $3 \times 3 \times 512$ filter dimension). Orientations of SRAMs are carefully adjusted so that controlling logic and PEs can be placed in the middle area, with reduced routing overhead. The current ASIC only contains 16 PEs. However, the vast die area with fillers (blue) suggests that a huge amount of extra PEs can be placed on the die, which should efficiently share the pool of SRAMs with the design methodologies introduced in Section 3. Estimates through Innovus imply an average power consumption of 55.4 mW on the die of 256 PEs and the same 18 SRAMs, which boosts the energy efficiency to 0.92 TOPs/W with further improvement possibilities.

From a functional perspective, the ASIC supports reconfiguration between standard convolution, max/min pooling, and full connection. Layer-wise kernel type, activation and filter dimension, nonlinear functions can also be reconfigured using ISA in Section 3.3.

As shown in Fig. 11, the testing board has been designed to integrate the socket of the CLCC84 chip package and FPGA interfacing with a host machine from Ref. [24]. The testing infrastructure is demonstrated in Fig. 12, where Python APIs are used to transmit/receive signals, and oscilloscopes are equipped for measuring signal voltages and core currents.

Regarding runtime power consumption, we measure the core current by deploying five layer neural networks, as shown in Fig. 13. It is observed that two convolutional layers incur long execution time and large current. Pooling layers have a relatively shorter time and smaller current, while the

Table 5. Runtime power consumption in mW for different phases and frequencies.

Frequency (MHz)	Initialize	Conv1	Pool1	Conv2	Pool2	FC	Idle	Avg. (conv1-fc)
30	1.92	2.84	2.58	3.04	2.71	3.32	1.92	2.62
60	3.32	5.29	4.76	5.47	5.09	5.74	3.32	4.71
100	5.19	8.56	7.67	8.71	8.26	8.97	5.19	7.51

Table 6. Comparison of physical properties with state-of-the-art designs.

Parameter	Eyeriss[28]	ENVISION[29]	Thinker[30]	This work	This work
Technology (nm)	65	28	65	65	65
Core area (mm^2)	12.25	1.87	19.36	3.24	3.24
Bit precision (b)	16	4/8/16	8/16	8	8
Num. of MACs	168	512	1024	16	256
Core frequency (MHz)	200	200	200	100	100
Performance (GOPS)	67.6	76	368.4	3.2	51.2
Power (mW)	278	44	290	7.51 (measured)	55.4 (estimated)
Energy efficiency	166.2 GOPS/W	1.73 TOPS/W	1.27 TOPS/W	426 GOPS/W	0.92 TOPS/W

FC layer has high power but a very short running time. Both initialization and idle phases consume similar currents. Table 5 shows the statistics of average power consumption for each operating phase under different running frequencies. At the design frequency of 100 MHz, the largest power value 8.97 mW is consumed by the FC layer, while the average power throughout operating phases of neural networks (form Conv1 to FC) is 7.51 mW, which implies the energy efficiency of 426 GOPs/W.

Table 6 shows a comparison between our work and other state-of-the-art works. Our taped-out IC with 16 PEs achieves the minimal measured power 7.51 mW among other designs, which is highly customized to ultra-low power applications. In contrast, the multi-threaded version with 256 PEs has the estimated energy efficiency of 0.92 TOPS/W, which is comparable to the state-of-the-art designs.

5. Conclusion

Neural networks have demonstrated tremendous success in a wide range of application domains, which drives research on specific AI accelerators in the past five years. Majority of customized AI accelerators targets convolutional neural network, while hybrid networks with non-standard layers have been purposed for applications beyond vision-based perception. In this work, we purpose a reconfigurable dataflow processor targeting multiple algorithmic kernels for both perception and control. Using the supported kernels, not only standard CNN but also compact CNN, ResNet, LSTM and deep reinforcement learning algorithms can be constructed.

The architecture is designed with a separate pool of PEs and SRAMs, whose functionalities are instantiated based on layer description through custom-designed ISA. Toolchains have been built to achieve compatibility with state-of-the-art AI programming framework. Experiments on profiling for three types of neural networks demonstrate the performance, resource utilization and special design features against the Intel processor. The taped-out ASIC under 65 nm UMC CMOS technology with 16 reconfigurable PEs is also demonstrated.

Future work includes optimization techniques regarding resource utilization, power consumption, reliability based on the design methodology. Further techniques to maximize resource sharing with low controlling overhead is the key to the enhancement of energy efficiency.

Acknowledgments

This work was supported by NSFC with Grant No. 61702493, 51707191, Science and Technology Planning Project of Guangdong Province with Grant No. 2018B030338001, the Key Field R & D Program of Guangdong Province (Grant No. 2019B010155003), Shenzhen S&T Funding with Grant No. KQJSCX20170731163915914, Basic Research Program No. JCYJ20170818164527303, JCYJ20180507182619669, and SIAT Innovation Program for Excellent Young Researchers with Grant No. 2017001.

References

[1] Chen Y, Krishna T, Emer J, et al. Eyeriss: An energy-efficient reconfigurable accelerator for deep convolutional neural networks. IEEE J Solid-State Circuits, 2017, 52, 127

[2] Jouppi N, Young C, Patil N, et al. In-datacenter performance analysis of a tensor processing unit. ACM/IEEE International Symposium on Computer Architecture, 2017, 1

[3] Chen Y, Tao L, Liu S, et al. DaDianNao: A machine-learning supercomputer. ACM/IEEE International Symposium on Microarchitecture, 2015, 609

[4] Cong J, Xiao B. Minimizing computation in convolutional neural networks. Artificial Neural Networks and Machine Learning, 2014, 281

[5] Yin S, Ouyang P, Tang S, et al. A high energy efficient reconfigurable hybrid neural network processor for deep learning applications. IEEE J Solid-State Circuits, 2017, 53, 968

[6] Russakovsky O, Deng J, Su H, et al. ImageNet large scale visual recognition challenge. Int J Comput Vision, 2015, 115, 211

[7] Iandola F, Han S, Moskewicz M, et al. SqueezeNet: AlexNet-level accuracy with 50x fewer parameters and < 0.5 MB model size. arXiv: 1602.07360, 2016

[8] Howard A, Zhu M, Chen B, et al. MobileNets: Efficient convolutional neural networks for mobile vision applications. arXiv: 1704.04861, 2017

[9] Simonyan K, Zisserman A. Very deep convolutional networks for large-scale image recognition. arXiv preprint arXiv:1409.1556, 2014,

[10] Yang C, Wang Y, Wang X, et al. A reconfigurable accelerator based on fast winograd algorithm for convolutional neural network in internet of things. IEEE International Conference on Solid-State and Integrated Circuit Technology, 2018, 1

[11] Vasilache N, Johnson J, Mathieu M, et al. Fast convolutional nets with fbfft: A GPU performance evaluation. arXiv: 1412.7580, 2014

[12] Guo K, Zeng S, Yu J, et al. A survey of FPGA-based neural network accelerator. arXiv: 1712.08934, 2017
[13] Mnih V, Kavukcuoglu K, Silver D, et al. Playing atari with deep reinforcement learning. arXiv: 1312.5602, 2013
[14] Mnih V, Kavukcuoglu K, Silver D, et al. Human-level control through deep reinforcement learning. Nature, 2015, 518, 529
[15] Silver D, Huang A, Maddison C, et al. Mastering the game of Go with deep neural networks and tree search. Nature, 2016, 529, 484
[16] Silver D, Schrittwieser J, Simonyan K, et al. Mastering the game of Go without human knowledge. Nature, 2017, 550, 354
[17] Chen Y, Emer J, Sze V. Eyeriss: A spatial architecture for energy-efficient dataflow for convolutional neural networks. ACM/IEEE International Symposium on Computer Architecture, 2016, 44, 367
[18] Gers F, Schmidhuber J, Cummins F. Learning to forget: Continual prediction with LSTM. 9th International Conference on Artificial Neural Networks, 1999, 850
[19] Basterretxea K, Tarela J, Del C. Approximation of sigmoid function and the derivative for hardware implementation of artificial neurons. IEE Proc Circuits, Devices Syst, 2004, 151, 18
[20] Sutton R, Barto A. Reinforcement learning: An introduction. MIT Press, 2018
[21] Gulli A, Sujit P. Deep learning with Keras. Packt Publishing Ltd, 2017
[22] Li S, Ouyang N, Wang Z. Accelerator design for convolutional neural network with vertical data streaming. IEEE Asia Pacific Conference on Circuits and Systems, 2018, 544
[23] Guo Y. Fixed point quantization of deep convolutional networks. International Conference on Machine Learning, 2016, 2849
[24] Opalkelly product manual. https://opalkelly.com/products/front-panel
[25] Chen W, Wang Z, Li S, et al. Accelerating compact convolutional neural networks with multi-threaded data streaming. IEEE Computer Society Annual Symposium on VLSI, 2019, 519
[26] MitchellSpryn solving a maze with Q learning. www.mitchell-spryn.com/2017/10/28/Solving-A-Maze-With-Q-Learning.html
[27] Liang M, Chen M, Wang Z. A CGRA based neural network inference engine for deep reinforcement learning. IEEE Asia Pacific Conference on Circuits and Systems, 2018, 519
[28] Chen Y, Krishna T, Emer J, et al. Eyeriss: An energy-efficient reconfigurable accelerator for deep convolutional neural networks. IEEE International Solid-State Circuits Conference (ISSCC), 2016, 127
[29] Moons B, Uytterhoeven R, Dehaene W, et al. ENVISION: A 0.26-to-10 TOPS/W subword-parallel dynamic-voltage-accuracy-frequency-scalable convolutional neural network processor in 28 nm FDSOI. IEEE International Solid-State Circuits Conference (ISSCC), 2017, 246
[30] Yin S, Ouyang P, Tang S, et al. 1.06-to-5.09 TOPS/W reconfigurable hybrid-neural-network processor for deep learning applications. Symposium on VLSI Circuits, 2017